Image feature analysis and computer-aided diagnosis in digital radiography. 2. Computerized determination of vessel sizes in digital subtraction angiography[a)]

Hiroshi Fujita,[b)] Kunio Doi,[c)] and Laura E. Fencil
Kurt Rossmann Laboratories for Radiologic Image Research, Department of Radiology, The University of Chicago, Chicago, Illinois 60637

Kok Gee Chua
Department of Medicine, The University of Chicago, Chicago, Illinois 60637

(Received 4 August 1986; accepted for publication 10 April 1987)

We developed an iterative deconvolution technique to determine the size of a "blurred" vessel in a digital subtraction angiographic (DSA) image by taking into account the unsharpness of the DSA system. Initially, a region of interest over a small segment of the contrast-filled vessel was selected in a DSA image, and the center line of the opacified vessel was determined by polynomial curve fitting of the locations of the peak pixel values along the vessel image. The blurred image profile was then obtained from pixel values across the vessel in a direction perpendicular to the center line. This measured profile was compared iteratively with a calculated profile for various size vessels, which was obtained from a cylindrical vessel model and from the line spread function, until the root-mean-square difference between the two profiles was minimized. The size of a cylindrical vessel yielding the matched profile was considered the best estimate of the unknown vessel size. Studies with a blood vessel phantom indicated that vessels larger than 0.5 mm could be measured with an accuracy and precision of approximately 0.1 mm, which is about 1/3 of the pixel size used in our DSA system. Details of our approach and some clinical vessel images with and without simulated stenotic lesions are presented.

Key words: digital subtraction angiography, image analysis, digital radiography

I. INTRODUCTION

Accurate measurement of vessel sizes for quantitative analysis of stenotic lesions is of great value in the assessment of regression or progression of vascular disease. The severity of stenotic lesions has traditionally been assessed by visual interpretation of angiograms in terms of percent stenosis. However, several studies have documented a large intra- and interobserver variability in the subjective visual evaluation of stenosis.[1–4] Detre *et al.*[1] reported that intraobserver agreement among 22 experienced angiographers on two cine viewings ranged from 9% to 72%. In addition, *postmortem* examinations have demonstrated a poor correlation between visual estimation of stenosis and subsequent pathologic findings.[5,6]

In order to reduce the uncertainty of subjective judgment of vessel narrowing and to provide a good estimate of the severity of stenoses, many investigators have devised methods for the quantitative analysis of (coronary) arteriograms which are based on digitized images and computer systems.[7–22] Brown *et al.*[9] developed a method for quantitative coronary angiography by employing two projected cinearteriographic views and by tracing the edges of coronary lesions. A limitation of their method is that the projected angiograms of the vascular segment have to be traced manually, and thus the key input data to be analyzed by a computer must still be based on a subjective visual interpretation. Sandor *et al.*[8,10] also determined, by hand, the shoulder portions of a blood vessel profile to estimate the vessel edge.

To overcome these manual procedures, Blankenhorn *et al.*[7] and Alderman *et al.*[11] determined the vessel size by using the vessel edges calculated from the maximum of the first derivative of the distribution of a vessel image. Because there was no reason why the actual vessel edge should correspond exactly to the pixel at the maximum of the first derivative, it was necessary to employ calibration curves, which can be obtained with the help of phantom measurements.[22] Reiber *et al.*[17] used the weighted sum of the first and second derivatives for this purpose; the weighting factor was determined empirically. Therefore, these methods contain the fundamental shortcoming that a somewhat arbitrary basis is assigned for determining the size of an unknown vessel, the image of which is degraded by the resolution properties of the imaging system. Imaging system unsharpness degrades the final image and consequently, hinders edge detection by man or by computer. The problem is compounded by the fact that a severely narrowed blood vessel segment is affected more by the blurring than is a normal segment.

Sandor *et al.*,[8,10] Nichols *et al.*,[15] Kruger *et al.*,[12,19] Jaques *et al.*,[18] and Seibert *et al.*[20] integrated the image distribution to determine the vessel size and/or the relative degree of stenosis. One of the limitations of this technique, in which the density (or pixel) values are summed over a cross section of the vessel, is the requirement for radiographic projections in which the x-ray beam is directed at right angles to the long axis of the artery. In fact, Jaques *et al.*[18] reported that the tilt of the vessel in relation to the x-ray beam resulted in significant error. Simons *et al.*[19] described the need for correction

 0094-2405/87/040549-08$01.20

factors, since the pixel value across an opacified vessel was not proportional to the iodine concentration multiplied by the vessel thickness.

Gould *et al.*[21,22] emphasize in their recent articles that in order to provide a measure of the net change of final, cumulative-hemodynamic characteristics of the stenosis, it is important to understand how functional effects of a stenosis relate to its anatomic geometry. Based on the fluid dynamic equations for flow in rigid tubes, the pressure drop across a coronary artery stenosis has been formulated by incorporating the blood flow and two constants, namely, the viscous pressure loss coefficient and the expansion pressure loss coefficient, both of which are related to the geometric characteristics of the stenosis.[21,22] Therefore, it is important to determine accurately the absolute dimensions, length, and shape of the stenotic lesions.

We have developed a new technique for determining the absolute size of a normal or narrowed blood vessel by taking into account the unsharpness of the digital imaging system. In order to implement our new approach in a digital subtraction angiographic (DSA) system, we measured the line spread function (LSF) and the characteristic curve of the system. Below, we describe the overall scheme for automated vessel-size estimation and the results obtained with a vessel phantom and with clinical DSA images.

II. MATERIALS AND METHODS

A. Iterative deconvolution technique

It is well known from basic imaging theory that the relationship between the input x-ray pattern (opacified vessel), the LSF (blurring effect of imaging system), and the final image (angiogram) is given by a convolution integral.[23,24] Doi *et al.* have shown previously by using computer simulation[25–27] that the image distribution (or profile) of a blood vessel filled with a contrast medium can be calculated by use of successive convolution integrals of the input profile of the vessel with the LSF's of geometric unsharpness and of the screen–film recording system. Experimental results were found to be in good agreement with calculated predictions.[28] These results imply that it is theoretically possible to derive the input x-ray pattern if both the LSF and the final image profile are known. In the present study, therefore, we applied this fundamental concept of the convolution relationship to find a solution for an unknown vessel size in the angiographic digital image analysis of stenotic lesions. Mathematically, an approach to solving this type of problem is the process called deconvolution. Because there are no simple analytical solutions to the deconvolution problem, we use computer simulation to determine a calculated image profile which will best fit the actual image profile obtained from an angiogram. The best fit of an image profile is determined by an iterative comparison of the calculated image profile with the actual result. Therefore, we shall call this approach an "iterative deconvolution" technique.

The effect of the unsharpness of a DSA imaging system on the image profile of a small vessel 0.5 mm in diameter is demonstrated in Fig. 1. The dashed curve represents the input pattern of the vessel, which corresponds to the image profile obtainable if an ideally sharp imaging system is employed. The solid curve represents the blurred image profile of the vessel, which was obtained by convolution of the input pattern (dashed curve) with the LSF (shown in Fig. 5). Generally, the smaller the vessel diameter, the larger the relative blurring effect on the image profile. For a given blurred image profile, our task is to find the size of an input vessel.

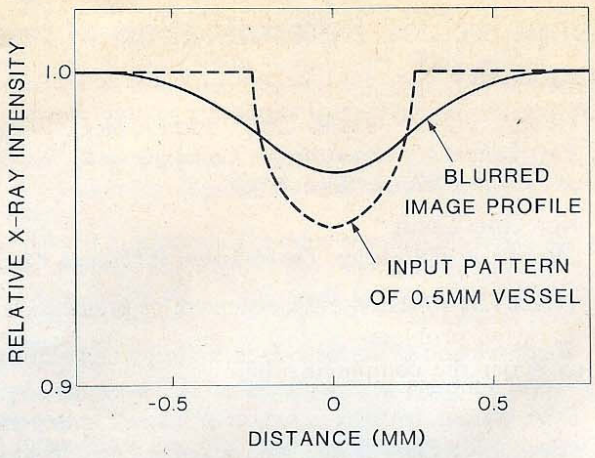

FIG. 1. Illustration of the effect of unsharpness of a DSA imaging system on the vessel image profile. The blurred image profile of a 0.5-mm vessel was obtained by convolution of the input pattern of the vessel with the line spread function shown in Fig. 5.

Figure 2 illustrates an essential part of our iterative deconvolution technique. The input vessel pattern is determined by assuming that a parallel x-ray beam is incident on a cylindrical vessel filled with a contrast material; the effect of the cylindrical-vessel model on measured vessel sizes will be discussed later. The calculation of the transmitted x-ray pattern takes into account the x-ray path length in the vessel and an effective attenuation coefficient of the opacified vessel, which is estimated from the contrast of the measured image profile and the approximate size of the vessel. This estimation is valid, because the normalized shape of the input x-ray pattern does not change with a small change in the effective attenuation coefficient. The computed image profile is ob-

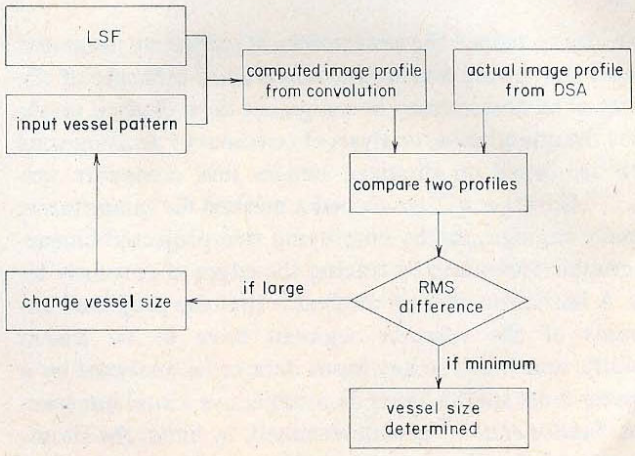

FIG. 2. Block diagram of an essential part of our iterative deconvolution technique for the determination of vessel sizes.

tained by convolution of this input pattern with the LSF, and then by conversion of relative x-ray intensities to DSA pixel values by means of the characteristic curve of the DSA system. When the image contrast is relatively small, however, this conversion can be approximated by a linear relationship, the proportionality constant of which is given by the gradient of the characteristic curve. The computed profile is compared iteratively with the actual image profile obtained from the DSA image by changing the cylindrical vessel size (the input pattern), until the root-mean-square (rms) difference between the two profiles is minimized. For this comparison, the area under the computed profile is normalized to be equal to that of the actual profile; this normalization corresponds to the condition that the cross-sectional area of the cylindrical vessel is equal to that of the actual vessel. The vessel size yielding the matched profile is considered the best estimate of an unknown vessel size. The dependence of the rms difference between profiles on the vessel size is demonstrated in Fig. 3. It should be noted that the relationship between the rms difference and the vessel size contains a sharp minimum, and that the vessel size is changed in increments of 0.1 mm. Since a circular cross section is assumed for the calculation of the input x-ray pattern, the vessel size yielding the minimum rms difference corresponds to an equivalent diameter of a cylindrical vessel having a cross-sectional area equal to that of an actual vessel.

Figure 4 shows the overall scheme for the computerized determination of vessel sizes from a DSA image. First, an operator selects an ROI (region of interest) over a small segment of a vessel image. All of the following calculations are performed automatically. The center line of the opacified vessel is determined by polynomial curve-fitting of the locations of the peak pixel values along the vessel image. The vessel image is then straightened[13,16,22] by conversion of the curved coordinates (center line versus its perpendicular lines) to the Cartesian coordinates so that image profiles along the curved vessel in a direction perpendicular to the center line are obtained from pixel values in a direction perpendicular to the straightened center line. For each image profile, a correction for nonuniform background is made

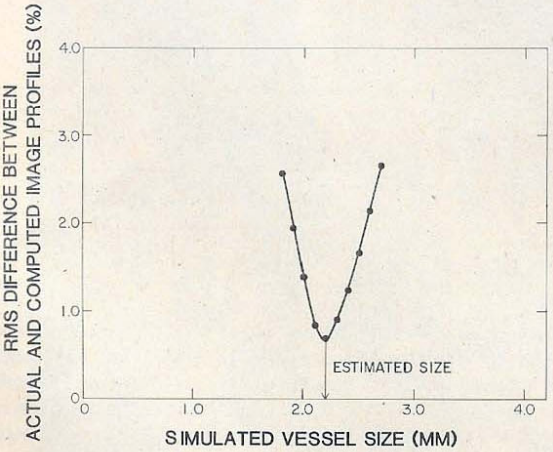

FIG. 3. Dependence of rms difference between actual and computed image profiles on simulated vessel size. The estimated size can be determined from the vessel size yielding the minimum rms difference.

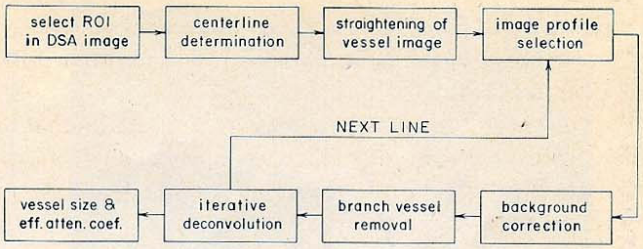

FIG. 4. Block diagram illustrating the overall scheme for the determination of vessel sizes in a selected segment of a DSA image. All of the calculations following the ROI selection are performed automatically.

(based on the linear fit of the backgrounds on both sides of the vessel when the nonuniformity is within a $\pm$ 3% difference). When the background is nonuniform (more than $\pm$ 3% difference in pixel values on the two sides), it is likely that a branch, or an overlapping or neighboring vessel, is located near the vessel of interest. Therefore, the computed image profile is matched, by the iterative deconvolution technique, only to the main part of the actual image profile, without correction of the background nonuniformity (or by removing the branch or neighboring vessel). The relative effective attenuation coefficients of the opacified vessel are also determined from the measured vessel size and from the contrast of the corresponding input profile. It should be noted that only *relative* effective attenuation coefficients can be obtained at present with our technique, because the orientation of the vessel relative to the image intensifier (II) input plane is not known in a single-plane technique, and because scatter and veiling glare are included in DSA images. Note also that the tilted cylindrical vessel is equivalent to a non-tilted cylindrical vessel with an increased effective attenuation coefficient, and therefore the accuracy of the measured size with our technique will be essentially independent of the vessel orientation. After the vessel sizes and the relative effective attenuation coefficients are determined line by line from the straightened image, the estimated sizes are displayed along the vessel image.

B. Experimental conditions

The DSA images in this study were obtained with a Digitron 2 system (Siemens Gammasonics, Des Plaines, IL). This system includes a triple-mode (25, 17, and 12 cm) Optilux RBV 25/17 HN CsI II (Siemens Medical Systems, Iselin, NJ) with grid (12:1, 40 lines/cm), coupled to a Siemens Videomed N TV system, and an x-ray tube with a nominal focal spot size of 0.6 mm. All images were acquired in the pulsed x-ray exposure mode, with an image matrix size of 512$\times$512. The raw data from the Digitron 2 were analyzed with a VAX 11/750 computer (Digital Equipment Corporation, Maynard, MA).

The pixel size (sampling distance), the characteristic curve, the modulation transfer function (MTF), and the LSF of our DSA system were measured in order to implement our approach to quantifying stenotic lesions in DSA systems. We used a square mesh phantom to measure the pixel size, which was needed for the determination of the MTF and the vessel size. The pixel size at the II input plane was approximately 7% greater in the horizontal direction

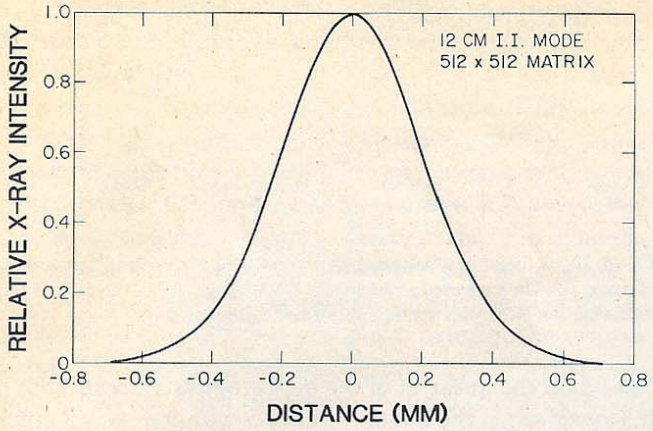

FIG. 5. Presampling analog LSF, which includes both the unsharpness of an II–TV digital system and the effect of the sampling aperture. The LSF was derived from the inverse Fourier transform of the presampling analog MTF. The pixel size is approximately 0.32 mm.

(parallel to the TV raster lines) than in the vertical direction for all II modes. However, for simplicity, we used the average of the two values. The pixel sizes were 0.32, 0.38, and 0.59 mm for the 12-, 17-, and 25-cm II modes, respectively. In a DSA system, the characteristic curve relates the output pixel values to the input x-ray intensities incident on the II,[29] and we used this curve to linearize the system response. The "presampling" analog MTF,[30,31] which includes both the unsharpness of an II–TV system and the effect of the sampling aperture, was obtained from the digital optical transfer functions determined with center and half-pixel-shifted alignments of the slit relative to the digital-sampling pixel. The presampling analog MTF measured with the slit in a direction parallel to TV raster lines was greater than that in the perpendicular direction; they were averaged for simplicity. The presampling analog LSF was then derived from the inverse Fourier transform of the presampling analog MTF, and shown in Fig. 5 for the 12-cm II mode. The methods of measurement and the experimental results for the characteristic curve[29] and the MTF[31] in II–TV digital imaging (DSA) systems are described in detail elsewhere.

In order to determine the accuracy and precision of our technique, we fabricated a vessel phantom consisting of polyethylene tubes of various diameters, ranging from 0.5 to 6.5 mm (i.d.); the actual tube sizes, which are regarded as "true" diameters, were measured with direct x-ray film and a magnifying glass. The concentration of the contrast medium, Renografin-76 (meglumine and sodium diatrizoate), in the tubes was varied from 8.8% to 100% (370 mg/ml iodine) in order to investigate the relationship between the relative effective attenuation coefficient of the opacified vessel and the concentration. All phantom images were acquired at 63 kV and in the 12-cm II mode, with a 12-cm Lucite block.

A simulated stenotic lesion was artificially produced using computer simulation by assuming that approximately one-half of an ellipsoid was attached inside the cylindrical vessel and thus removed the contrast medium from the vessel occupied by this lesion. First, the two-dimensional profile of a simulated stenotic lesion was calculated from the relative effective attenuation coefficient of the opacified vessel and the geometric parameters (diameter and length) of the lesion. A blurred profile of this lesion was determined by using the LSF of the DSA system and then superimposed on one side of the edges in a clinical image and also in images of the vessel phantom. With this method, one can create a simulated lesion having a known percent area stenosis; we used this for comparison with the measurements which we made with the iterative deconvolution technique.

III. RESULTS

Figure 6 demonstrates the comparison between actual and calculated image profiles. These image profiles can be displayed on a CRT monitor, if desired, during our computerized analysis of vessel sizes for monitoring of the procedure. An actual image profile, which was obtained from a certain location in the selected ROI on a DSA image of a vessel

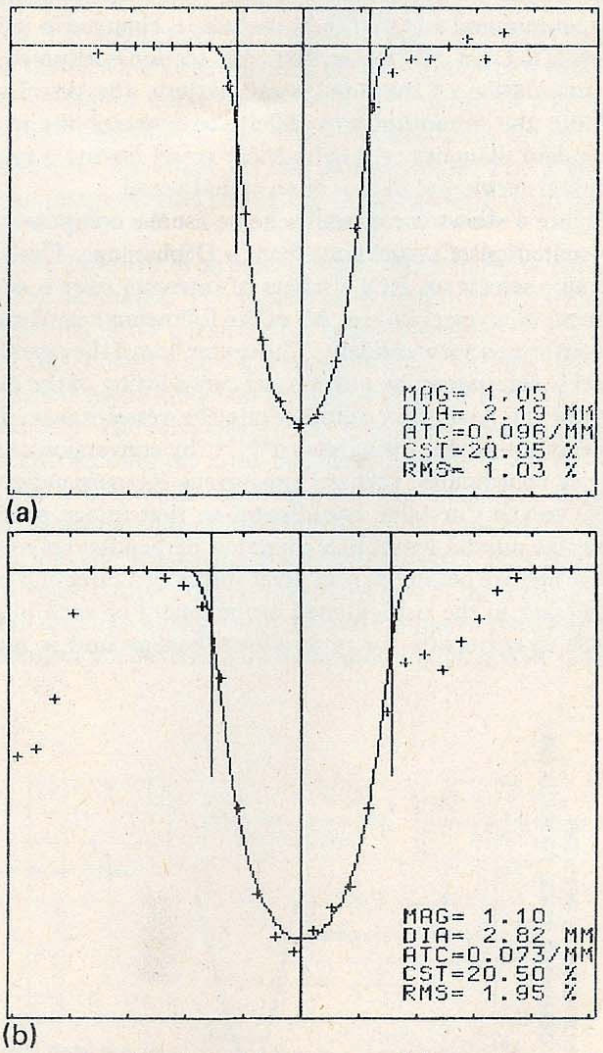

FIG. 6. Image profiles obtained from (a) a vessel phantom image and (b) a clinical image with a partially overlapping branch vessel. The actual image profile obtained from the straightened image is shown by the symbol +, and the computed "matched" image profile is shown by the solid curve. The two vertical lines near the edges of the profiles show the vessel size determined with our method. The magnification factor (MAG), measured diameter in the object plane (DIA), relative effective attenuation coefficient (ATC), image contrast (CST), and root-mean-square difference between the actual and computed image profiles (rms) are shown in the lower right.

phantom, and the computed "matched" image profile are shown by crosses and a solid curve, respectively, in Fig. 6(a). It is apparent that the computed image profile agreed well with the actual image profile. The two vertical lines near the edges of the profile show the vessel size determined by our method. It should be noted that the positions of these vertical lines are by no means related in a simple way to the edges of the profiles; this is due to the effect of unsharpness of the imaging system. The actual image profile shown in Fig. 6(b) partially overlaps a branch vessel (on the right-hand side of the profile). However, our algorithm can ignore data points due to the branch vessel, and the computed profile is compared only with the major part of the actual profile in question.

In Fig. 7, the selected ROI is indicated by a rectangular white box on a curved vessel image, and the straightened vessel image is in another white box. Measured vessel sizes are plotted as dark dots on the image in both rectangles for visual comparison. Figure 8 demonstrates the removal of branch vessels and/or overlapping vessels in an intracranial DSA image. The image in the selected ROI was expanded three times in Fig. 8, since our results are more accurate than the pixel size by a factor of 3, as will be discussed below. For small segments of DSA images, as illustrated in Figs. 7 and 8, the computation time for determining vessel sizes is approximately 1 min.

Figure 9 shows a comparison of measured diameters of the iodinated plastic tubes in the vessel phantom with their "true" diameters. The error bars correspond to the standard deviation derived from measurements on tubes with different iodine concentrations and also from repeated measurements on different images obtained with independent exposures. It is obvious that the measured vessel diameters agree well with true diameters, despite a considerable variation in the concentration of the contrast medium employed in the phantom. It should be noted also that no correction factors and no calibration curves are required with our iterative deconvolution technique. For tube sizes greater than 0.5 mm, the accuracy and precision are approximately 0.1 mm, which is about 1/3 of the pixel size used. This result seems encouraging, since it indicates that certain quantitative data in a digital imaging system can be obtained with an accuracy less than the pixel size used. In Fig. 10, the relative effective attenuation coefficients of opacified vessels determined for three different tube sizes are plotted against the concentration of the contrast medium. Note that the attenuation coefficient of an opacified vessel is ideally equal to the product of the iodine attenuation coefficient and the iodine concentration. The measured coefficients correlate approximately lin-

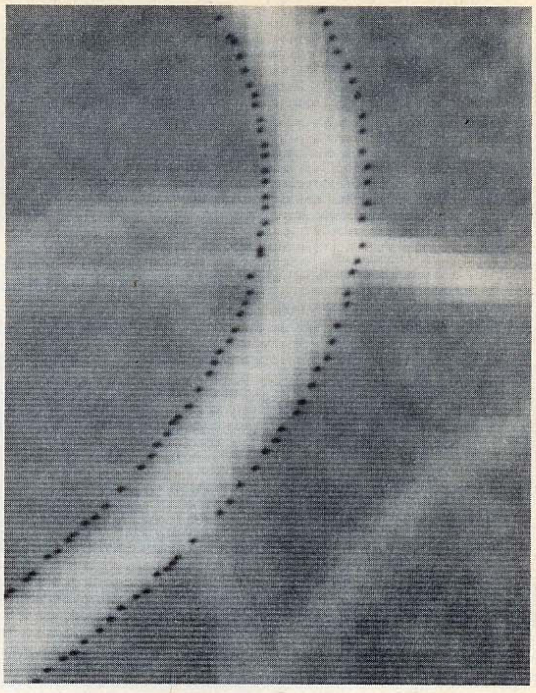

FIG. 8. An image expanded three times, illustrating measured sizes along the selected vessel segment and also the removal of branch vessels and overlapping vessels in an intracranial DSA image.

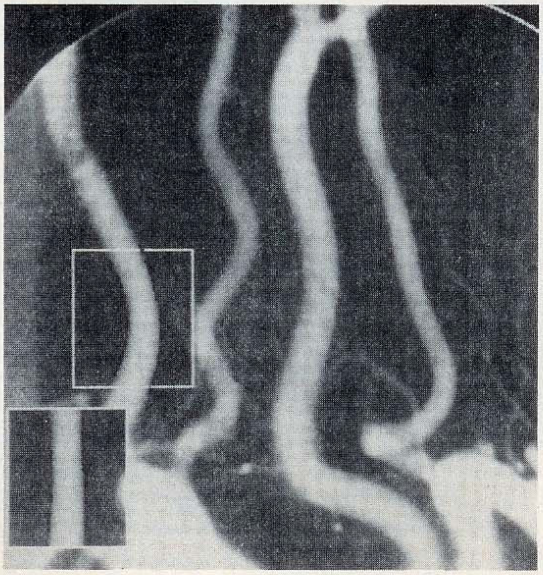

FIG. 7. The curved vessel image in a selected ROI is straightened as shown in lower left. Measured sizes are marked by dark dots.

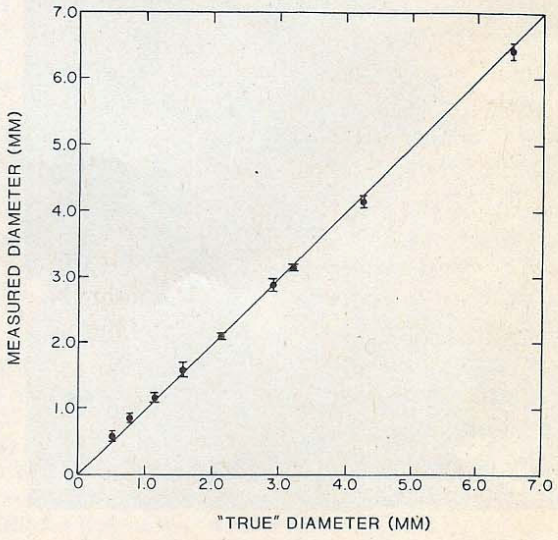

FIG. 9. Comparison of measured diameters of iodinated plastic tubes in the vessel phantom with their true diameters. For tube sizes greater than 0.5 mm, the accuracy and precision are approximately 0.1 mm each.

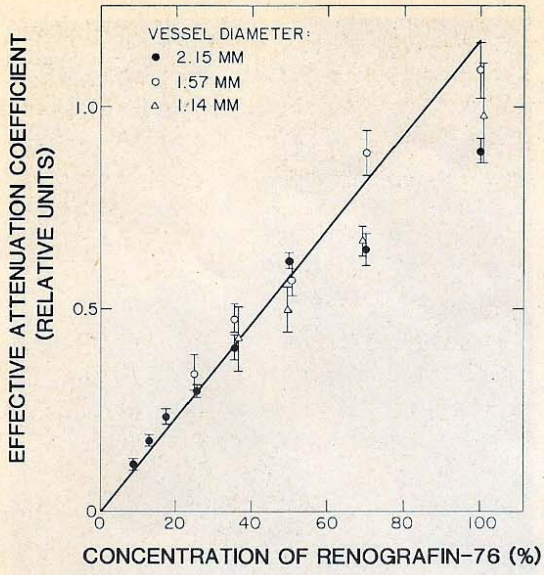

FIG. 10. Relationship between relative effective attenuation coefficient of the opacified vessel and concentration of the contrast medium.

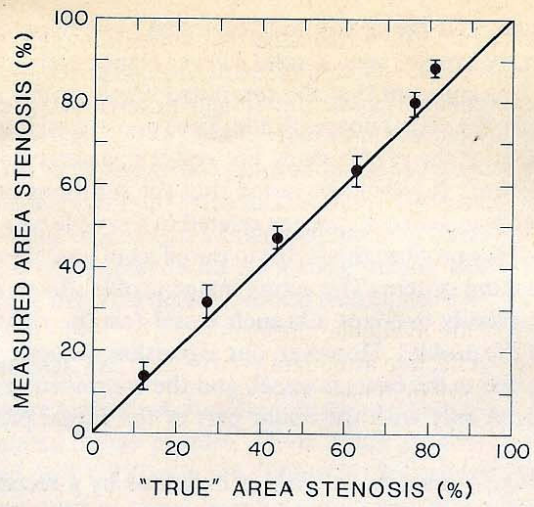

FIG. 12. Comparison of measured percent area stenoses, which was produced artificially on the vessel phantom image, with the true percent area stenoses created in a 6.5-mm vessel.

early with the concentration of Renografin-76, except at high concentrations. However, this correlation is considerably poorer than that obtained for vessel diameters (Fig. 9). The deviation of the data points at high concentrations is probably due to the effects of veiling glare,[32,33] scattered radiation, and beam hardening. In addition, the experimental error for the relative effective attenuation coefficient is expected to be greater than that for the vessel size, because two experimental values, i.e., the size and contrast of the vessel, are required for determining the attenuation coefficient.

Figure 11 (image expanded three times) illustrates the analysis of the image of a stenotic lesion which was artificially produced in a normal high-contrast, large vessel obtained with a clinical DSA image. The graph in Fig. 11 shows the measured vessel size along the center line of the selected vessel. The percent area stenosis created was 68%. The percent area stenosis measured with our technique was 67%. In addition, we verified that the artificial stenoses produced in phantom images of a 6.5-mm vessel agreed well with measurements over a wide range of values of percent stenosis, as shown in Fig. 12. These results indicate the effectiveness of our technique in the determination of sizes of stenotic lesions.

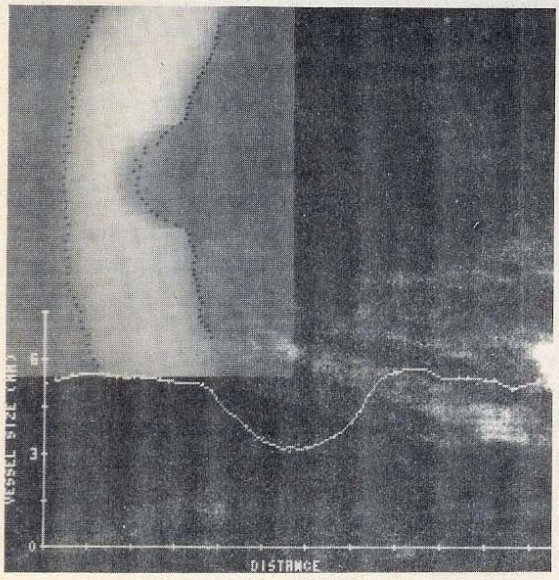

FIG. 11. Illustration of the analysis of a simulated stenotic lesion (68%), which was produced artificially in a clinical DSA image of a normal vessel. The percent area stenosis measured by our technique was 67%.

IV. DISCUSSION

An advantage of our technique is that all image profile data are directly utilized for the determination of an unknown vessel size. Thus, even though DSA images have problems such as quantum mottle, a limited number of data points, and background nonuniformities, it becomes possible to assess the severity of stenotic lesions accurately. However, all previously described methods depend on only a fraction (or a sum) of the available image profile data, such as edge configurations or first derivatives. Based on this unique advantage of our method and on the ability to compensate for the unsharpness of the imaging system, we believe that the severity of stenotic lesions can be assessed more accurately with our method than with any others available at present.

The assumption which we made in our current technique is that the cross section of the blood vessel is circular, assumption which appears not to be valid for an eccentric stenotic lesion and vessels of irregular shape. However, as shown in Figs. 11 and 12, it seems that the area of the eccentric cross section in the obstructed vessel can be well represented by the equivalent area of the circular cross section in the calculated cylindrical vessel. At the narrowed region in Fig. 11, the measured size shown by the black dots is slightly larger than the apparent borders of the lesion; this implies that the vessel size will be underestimated if only the edges are taken into account. Another model often used in the determination of sizes of blood vessels is a cylinder having different diameters in orthogonal directions, i.e., an elliptical

cross section.[9,22] The use of the biplane technique based on the elliptical model is generally expected to provide a more reliable estimate of the severity of stenotic lesions than does the single-plane technique with the circular model. Our iterative deconvolution technique can also be applied to the analysis of biplane angiograms with the elliptical model; however, the usefulness of this approach remains to be investigated.

With our technique, additional image data along the vessel segment are available; these include the vessel contrast, the relative effective attenuation coefficient, and the sum of image profile data. These data can be applied to the determination of the size of the vessel (or one of the two diameters for the elliptical vessel), as has been done by some investigators.[12,15,18] However, we did not use these data at present, because the orientation of the vessel segment relative to the II input plane is unknown and thus the results could be inaccurate. We believe, however, that it will be helpful to apply these data to blood flow analysis, and also to the determination of the two diameters of an elliptical vessel when a stereoscopic DSA system is employed.

To reduce the computation time, one can replace the convolution integral with the fast Fourier transform (FFT) algorithm, because the computation in the frequency domain can be performed more quickly than that in the spatial domain. In this case, the MTF of our DSA system would be employed together with the Fourier spectrum of the input x-ray pattern,[23,24] and the Fourier spectrum of an actual image would be compared iteratively with the Fourier spectrum of a computed image profile.

In clinical practice, one of the important factors affecting the accuracy of the computer-determined absolute vessel dimensions is the reliable measurement of the geometric magnification. The final vessel dimension is obtained by dividing the measured vessel size by the magnification factor. With our current technique, the magnification factor of the vessel needs to be estimated from the approximate geometric relationship among the vessel, the II input plane, and the x-ray tube focal spot; the accuracy of this estimate may not be very high, however. Brown *et al.*[9] determined this magnification factor for quantitative coronary arteriography by using the catheter tip as a scaling device. This technique may not be applicable to most DSA examinations, because the catheter tip is usually placed at some distance from the stenotic lesion and thus is not included in the image. In addition, the magnification factor of the vessel of interest in a plane parallel to the II input plane may not be the same as that of the catheter tip. One potential alternative approach is the application of the stereoscopic or biplane technique, in conjunction with an appropriate calibration procedure for the three-dimensional coordinate system[34] with which the stenotic vessel is located.

In conclusion, we developed an iterative deconvolution technique to determine the size of a blurred vessel in a DSA image by taking into account the unsharpness of the DSA system. The measured size corresponds to the diameter of an equivalent cylindrical vessel which has the same cross-sectional area as that of the blurred vessel. Phantom studies showed that vessel sizes greater than 0.5 mm can be measured with an accuracy and precision of approximately 0.1 mm, which is about 1/3 of the pixel size used. We believe that our technique will be useful for measuring the vessel size accurately and thus for assessing the severity of stenotic lesions; we also believe that it will be applicable to the measurement of the blood flow characteristics as well as to investigations of the relationship between the anatomic and functional severity of stenotic lesions.[21,22]

ACKNOWLEDGMENTS

We are grateful to Dr. E. E. Duda, Dr. A. S. Muraki, Dr. K. Ohara, Dr. M. L. Giger, Dr. H.-P. Chan, and Dr. K. R. Hoffmann for their discussions; to Mr. K. Katafuchi for his contribution to fabricating the phantoms; to Miss E. Ruzich for her secretarial assistance; and to Mrs. E. Lanzl for editing the manuscript. This work was supported by USPHS Grants CA 24806 and T32 6M07281.

[a] This paper was presented at the 71st Scientific Assembly and Annual Meeting of the Radiological Society of North America, Chicago, IL, 17–22 November 1985.

[b] Present address: Department of Electrical Engineering, Gifu Technical College, Motosu, Gifu, 501-04, Japan.

[c] Address reprint requests to: Kunio Doi, Ph.D., Department of Radiology, Box 225, The University of Chicago, 5841 South Maryland Avenue, Chicago, IL 60637.

[1] K. M. Detre, E. Wright, M. L. Murphy, and T. Takaro, "Observer agreement in evaluating coronary angiograms," Circulation **52**, 979 (1975).

[2] L. M. Zir, S. W. Miller, R. E. Dinsmore, J. P. Gilbert, and J. W. Harthorne, "Interobserver variability in coronary angiography," Circulation **53**, 627 (1976).

[3] T. A. DeRouen, J. A. Murray, and W. Owen, "Variability in the analysis of coronary arteriograms," Circulation **55**, 324 (1977).

[4] M. E. Sanmarco, S. H. Brooks, and D. H. Blankenhorn, "Reproducibility of a consensus panel in the interpretation of coronary angiograms," Am. Heart J. **96**, 430 (1978).

[5] Z. Vlodaver, R. French, R. A. Van Tassel, and J. E. Edwards, "Correlation of the *antemortem* coronary arteriogram and the *postmortem* specimen," Circulation **47**, 162 (1973).

[6] C. M. Grondin, I. Dyrda, A. Pasternac, L. Campeau, M. G. Bourassa, and J. Lesperance, "Discrepancies between cineangiographic and *postmortem* findings in patients with coronary artery disease and recent myocardial revascularization," Circulation **49**, 703 (1974).

[7] D. H. Blankenhorn, S. W. Brooks, R. H. Selzer, D. W. Crawford, and H. P. Chin, "Assessment of atherosclerosis from angiographic images," Proc. Soc. Exp. Biol. Med. **145**, 1298 (1974).

[8] S. Paulin and T. Sandor, "Densitometric assessment of stenoses in coronary arteries," Proc. SPIE **70**, 337 (1975).

[9] B. G. Brown, E. Bolson, M. Frimer, and H. T. Dodge, "Quantitative coronary arteriography: Estimation of dimensions, hemodynamic resistance, and atheroma mass of coronary artery lesions using the arteriogram and digital computation," Circulation **55**, 329 (1977).

[10] T. Sandor, A. V. Als, and S. Paulin, "Cine-densitometric measurement of coronary arterial stenoses," Catheterization Cardiovasc. Diagn. **5**, 229 (1978).

[11] E. L. Alderman, L. E. Berte, D. C. Harrison, and W. Sanders, "Quantitation of coronary artery dimensions using digital image processing," Proc. SPIE **314**, 273 (1981).

[12] R. A. Kruger, "Estimation of the diameter and iodine concentration within blood vessels using digital radiography devices," Med. Phys. **8**, 652 (1981).

[13] B. G. Brown, E. L. Bolson, and H. T. Dodge, "Arteriographic assessment of coronary atherosclerosis: Review of current methods, their limitations, and clinical applications," Arteriosclerosis **2**, 2 (1982).

[14] J. R. Spears, T. Sandor, A. V. Als, M. Malagold, J. E. Markis, W. Grossman, J. R. Serur, and S. Paulin, "Computerized image analysis for quantitative measurement of vessel diameter from cineangiograms," Circulation **68**, 453 (1983).

[15]A. B. Nichols, C. F. O. Gabrieli, J. J. Fenoglio, and P. D. Esser, "Quantification of relative coronary arterial stenosis by cinevideodensitometric analysis of coronary arteriograms," Circulation **69**, 512 (1984).
[16]J. H. C. Reiber, C. J. Kooijman, C. J. Slager, J. J. Gerbrands, J. C. H. Schuurbiers, A. Den Boer, W. Wijns, and P. W. Serruys, "Computer assisted analysis of the severity of obstructions from coronary cineangiograms: A methodological review," Automedica **5**, 219 (1984).
[17]J. H. C. Reiber, C. J. Kooijman, and C. J. Slager, J. J. Gerbrands, J. C. H. Schuurbiers, A. Den Boer, W. Wijns, p. W. Serruys, and P. G. Huggenholtz, "Coronary artery dimensions from cineangiograms: Methodology and validation of a computer-assisted analysis procedure," IEEE Trans. Med. Imag. **3**, 131 (1984).
[18]P. Jaques, F. DiBianca, S. Pizer, F. Kohout, L. Lifshitz, and D. Delany, "Quantitative digital fluorography: Computer versus human estimation of vascular stenoses," Invest. Radiol. **20**, 45 (1985).
[19]M. A. Simons and R. A. Kruger, "Vessel diameter measurement using digital subtraction radiography," Invest. Radiol. **20**, 510 (1985).
[20]J. A. Seibert, D. P. Link, H. H. Hines, and H. A. Baltaxe, "Videodensitometric quantitation of stenosis: *In vitro* and *in vivo* validation," Radiology **157**, 807 (1985).
[21]K. L. Gould, "Quantification of coronary artery stenosis *in vivo*," Circ. Res. **57**, 341 (1985).
[22]W. H. Wong, R. L. Kirkeede, and K. L. Gould, "Computer applications in angiography, in *Cardiac Imaging and Image Processing*, edited by S. M. Collins and D. J. Skorton (McGraw–Hill, New York, 1986), pp. 206–238.
[23]K. Doi and K. Rossmann, "X-ray images of small blood vessels in angiography: Question of isoplanatism," Med. Phys. **2**, 301 (1975).
[24]C. E. Metz and K. Doi, "Transfer function analysis of radiographic imaging systems," Phys. Med. Biol. **24**,1079 (1979).
[25]K. Doi and K. Rossmann, "Computer simulation of small blood vessel imaging in magnification radiography," in *Small Vessel Angiography*, edited by S. K. Hilal (Mosby, St. Louis, MO, 1973), pp. 6–12.
[26]K. Doi and K. Rossmann, "The effect of radiographic magnification on blood vessel imaging with various screen–film systems," Med. Phys. **1**, 257 (1974).
[27]K. Doi and K. Rossmann, "Effect of focal spot distribution on blood vessel imaging in magnification radiography," Radiology **114**, 435 (1975).
[28]K. Doi and K. Rossmann, "Validity of computer simulation of blood vessel imaging in angiography" Med. Phys. **4**, 400 (1977).
[29]H. Fujita, K. Doi, M. L. Giger, and H. P. Chan, "Investigation of basic imaging properties in digital radiography. 5. Characteristic curves of II–TV digital systems," Med. Phys. **13**, 13 (1986).
[30]M. L. Giger and K. Doi, "IInvestigation of basic imaging properties in digital radiography. 1. Modulation transfer function," Med. Phys. **11**, 287 (1984).
[31]H. Fujita, K. Doi, and M. L. Giger, "Investigation of basic imaging properties in digital radiography. 6. MTF's of II–TV digital imaging systems," Med. Phys. **12**, 713 (1985).
[32]J. A. Seibert, O. Nalcioglu, and W. Roeck, "Removal of image intensifier veiling glare by mathematical deconvolution techniques," Med. Phys. **12**, 281 (1985).
[33]O. Nalcioglu, W. Roeck, J. A. Seibert, S. Thomas, and C. Orton, in *Digital Radiography*, edited by J. Kereiakes and Thomas (Plenum, New York, 1985), pp. 83–132.
[34]S. A. MacKay, M. J. Potel, and J. M. Rubin, "Graphics methods for tracking three-dimensional heart wall motion," Comp. Biomed. Res. **15**, 455 (1982).